Hindawi
International Transactions on Electrical Energy Systems
Volume 2023, Article ID 6604487, 18 pages
https://doi.org/10.1155/2023/6604487

Research Article

Backstepping Controller Design for Power Quality Improvement in a Two-Stage Grid-Connected Photovoltaic Systems with LCL Filter

Isaac Fredy Bendé,[1] Etienne Tchoffo Houdji,[1] Guy Bertrand Tchaya,[1] Jean Luc Dit Bouerdjila Nsouandélé,[1] Martin Kamta,[2] and Haman-Djalo[3]

[1]*Department of Renewable Energy, National Advanced School of Engineering of Maroua, University of Maroua, Maroua, Cameroon*
[2]*Department of Electrical, Energetic and Automatic Engineering, National School of Agro-Industrial Sciences, University of Ngaoundere, Ngaoundere, Cameroon*
[3]*Department of Physics, Faculty of Science, University of Ngaoundere, Ngaoundere, Cameroon*

Correspondence should be addressed to Etienne Tchoffo Houdji; tchoffohoudji@gmail.com

Received 14 September 2022; Revised 9 November 2023; Accepted 13 November 2023; Published 23 November 2023

Academic Editor: Nitin Gupta

In a grid-connected photovoltaic system, the quality of energy injected by the photovoltaic system into the grid is directly linked to the topology of the inverter used and to the efficiency of its control technique. This paper addresses this problem for a two-level grid-connected photovoltaic inverter operating under low irradiance conditions. The aim is to reduce the harmonic distortion on the electrical network and therefore improve its power quality. To achieve this goal, a control strategy was set up considering the nonlinearity of the dynamic system, and the high dimension of the system model. Thus, a nonlinear controller designed using the backstepping technique is proposed. The effectiveness of this control strategy was evaluated by simulation in MATLAB/Simulink. Results show that the proposed control technique significantly improves the power quality of the grid-connected photovoltaic system by minimizing the current harmonic distortion rates in low irradiance conditions. The current harmonic distortion rates obtained for solar irradiance of 1000 W/m^2, 750 W/m^2, 500 W/m^2, and 250 W/m^2 are 0.48%, 0.78%, 1.22%, and 2.16%, respectively. The power factor is 0.988, and the DC bus voltage is maintained at its reference voltage of 600 V with a very low response time during the transient phases. A comparison of our simulation results with those found in the literature on other control techniques such as proportional-integral-derivative (PID) and synergetic controls shows the efficiency, superiority, and satisfactory performance of the proposed control scheme to minimize harmonic distortion under low irradiance conditions. The robustness and better dynamic performance of the proposed backstepping controller under varying irradiance conditions have also been shown.

1. Introduction

1.1. Background. Greenhouse gases are one of the most important sources of climate change. These greenhouse gases come mostly from the combustion of fossil fuels such as gas, oil, and coal. This combustion of fossil fuels produces an increase of up to 70% of greenhouse gases in the world, thereby causing global warming [1, 2]. One of the most urgent and inescapable solutions to this problem of global warming is to move to renewable energy sources by reducing the dependency of power system around the word on fossil fuels [3–7]. This is why the energy transition towards renewable energy sources has received more attention in recent years, in various sectors due to their great potential in the reduction of greenhouse gas emissions [4]. The main renewable energy sources are wind, biomass, hydroelectricity, geothermal energy, biofuels, and solar energy [5–8]. Advantages such as inexhaustibility, free of charge, and

cleanliness make photovoltaic solar energy one of the most dominant energy sources, and the best alternative to other existing renewable energy sources in terms of electricity supply [3, 9]. State governmental measures in many countries around the world leading to the reduction in the cost of the solar photovoltaic module by more than 40% have contributed to a rapid spread of photovoltaic (PV) systems in these countries [10]. A photovoltaic panel, also called photocell, enables the conversion of solar energy into direct electrical energy. Its production strongly depends on meteorological conditions especially, the irradiance and the ambient temperature [11, 12].

1.2. Challenges. To ensure the extraction of the maximum power in a photovoltaic system under variable irradiance and temperature, a Maximum Power Point Tracking (MPPT) algorithm is implemented through a DC-DC converter [13, 14]. The inverter can therefore convert this DC energy into AC form for AC loads [15]. Photovoltaic systems can be mainly classified into standalone and grid-connected photovoltaic systems [7, 16]. In the grid-connected PV systems, solar energy source is connected to the grid through inverters and these are used to fill the energy deficit of grids [15, 16]. During the coordination and operation of the grid-connected photovoltaic systems, undesirable effects on both the grid and end-user equipment can arise due to power quality disruptions due to the variations in meteorological conditions and the presence of nonlinear loads into the grid [17]. One of the main and worst power quality disturbances is the injection of harmonic distortions of the current by the solar photovoltaic systems and nonlinear loads into the grid [9, 18, 19], especially in low irradiance conditions [20, 21]. Disturbances caused by these harmonic distortions of the current in the electrical grid are overheating of cables, breakdown of capacitors, increase in line losses, power factor degradation, vibration and acoustic noise from motors, malfunction of metering devices, and aging of lines [15, 22]. To address the aforementioned problems, various control strategies are proposed in the literature by many authors.

1.3. Literature Review. Much attention have been paid to inverter control techniques to ensure sinusoidal waveform of the current with low THD, fast dynamic response, and invariable frequency of the system under different types of loads [23]. In their work, Yaïchi et al. have proposed the use of multilevel converters and thus allowing them to provide a multilevel wave with less total harmonic distortion depending on the number of switching cells [24]. However, this method requires more switches than conventional converters and thus makes these converters expensive and bulky. In order to minimize the THD, Imarazene et al. have proposed techniques of harmonics selection in which harmful harmonics from the frequency spectrum are selected and removed [25]. The major drawback of this solution is the difficulty to calculate the exact commutation angles. This leads to the complexity of the method and limits its feasibility. Mamane et al. have proposed an alternative to the abovementioned harmonics selection techniques. Their technique consists of a reactive power compensation algorithm applied to parallel active filters [26]. However, the use of this technique to improve of the power quality is often very bulky and expensive. Pesdjock et al. have proposed an improved variant of the associated classical synergetic control to reduce the THD of a grid-connected photovoltaic system [15]. In their approach, these authors have modified the traditional synergetic method by creating an intermediate virtual control. Sharma and Gali proposed a modified hysteresis current controller switching scheme for multifunctional (MHCC) grid-tied photovoltaic inverters [27]. Their control technique consists of feeding an active power to the local grid during day time and acting as a shunt active power filter (SAPF) to mitigate reactive power, current harmonics, and switching frequency problems. Morey et al. have recently proposed a review of the latest grid-connected inverter control techniques and associated inverters configurations [16]. The main control techniques for grid-connected inverters identified by these authors include the synchronous reference frame (SRF) theory, the double synchronous reference frame (DSRF) theory, the stationary two-phase reference frame theory, a combined action of the proportional resonance and the harmonic compensator (PR + HC) controllers based on stationary two-phase reference frame theory, and a combined action of a 3rd-order proportional resonance and proportional integral (PR + PI) controllers based on the theory of the stationary two-phase reference frame. Morey et al. have also discussed in depth control algorithm approaches based on synchronous reference frame (SRF) theory, IcosΦ, instantaneous symmetrical component theory, and instantaneous reactive power theory (IRPT), for controlling grid-connected PV inverters [28]. In addition to the abovementioned control techniques, several other techniques exist among which PID control [29–32] is applied to LCL filter, sliding mode control (SMC) [33], linear control [34], linear resonant control [35], Lyapunov control [36], and passivity-based control [37]. They are combined between them or with other modern control techniques in order to achieve better performances and power qualities of photovoltaic systems. Thus, Fanjip et al. [38] have applied the fuzzy logic control associated with the sliding mode control to a parallel active filter to eliminate harmonics distortion of the current in the same system as Pesdjock et al. [15]. Finally, for the above PV system, Lakshmi and Hemamalini have proposed the design of a control decoupled from the system using a fractional PI controller to minimize the harmonic distortions of the current [39]. Subsequently, Golzari et al. have proposed a direct predictive power control based on the Lyapunov function developed for the control of the three-phase grid-connected PV inverter [40]. This control technique based on the discrete first-order filter model aims to improve the tracking speed of the controller during rapid changes in solar irradiance. A nonlinear sliding mode controller called supertwisted integral sliding mode control has been proposed for a three-phase grid-connected inverter [41, 42]. This controller has proven to be robust and maintains low THD in the presence

of grid impedance variation, filter parameter drift, and network harmonic distortion. Adding the supertwisting action helps to remove the chattering problem associated with the conventional sliding mode control strategy, and the integral action helps to improve the steady-state error of the grid current. A proportional integral (PI) control strategy associated with repetitive control for grid-connected photovoltaic inverters with a third-order output filter has been proposed by Li et al. [43]. The proposed control scheme also improves the harmonic suppression ability of the PV inverter and the system maintains better stability and fast dynamic response. Deželak et al. have proposed a comparison between the particle swarm optimization (PSO) and Ziegler–Nichols (ZN) tuning methods for controlling the inverter of the grid-connected PV system with a third-order output filter [44]. These two approaches are generally used to determine the parameters of proportional integral (PI) controllers. The PSO-optimized PI controller shows its superiority over the ZN optimization technique in terms of system stability and power quality. A fuzzy-PI and a fuzzy sliding mode controller for two-stage single-phase photovoltaic inverters connected to the grid through a third-order filter are also proposed by Zeb et al. [45]. Their controllers regulate the DC link voltage and improve the power quality of the system.

One of the most used controllers for the grid-connected photovoltaic inverter is the backstepping controller. It can be used alone or associated with other controllers. Below are some relevant publications where this control strategy is used. Thus, a comparison between sliding mode, fuzzy logic, and backstepping controllers is presented by Zadeh et al. [46]. They found that backstepping was the best controller with the highest performance. A robust and nonlinear backstepping controller for inverters is proposed by Kolbasi and Seker [47]. However, this controller is hard to handle control because it contains more than two gains. Zouga et al. have proposed a backstepping controller based on the particle swarm optimization (PSO) algorithm for a three-phase grid-connected solar system [48]. The authors use the backstepping technique based on the L-filter model to develop three cascade controllers. The first one aims to fix the DC voltage of the PV panels at the MPP (maximum power point). The second controller is designed to inject a sinusoidal three-phase current into the grid through the control of an inverter. The third controller is a proportional integral (PI) controller based on the particle swarm optimization (PSO) technique, which aims to regulate the voltage of the intermediate circuit to a constant reference value. Pervej et al. have proposed a nonlinear backstepping controller for three-phase grid-connected PV systems based on the direct power controller (DPC) approach [49]. In their work, the internal current control loop is deleted; this simplifies the modeling of the grid-connected system by a first-order filter as well as the controller design by improving the transient performance. In order to improve dynamic stability and power quality, and control the appropriate amount of active and reactive power to be injected into the grid, nonlinear adaptive backstepping controllers for grid-connected three-phase PV systems through a first-order and LC filters have been proposed by Roy et al. [50, 51]. A filtered nonlinear adaptive backstepping controller to connect a solar PV system to the three-phase grid through a first-order filter has been proposed by Xu et al. [52]. This control strategy allows the regulation of the DC link voltage of the PV system and of the current used to control the active or reactive power injected into the grid. The technique also provides a solution to the intrinsic problem of differential expansion and saturation in the backstepping control technique by using a control filter to eliminate the impact of time derivative and saturation from the controller.

Other works in which LCL filters are used to eliminate harmonics distortions in grid-connected photovoltaic systems have been presented by various authors. For example, a hybrid controller incorporating repetitive and stateful pole assignment control for a three-phase grid-connected inverter with LCL filter has been proposed by Liu et al. [53]. A simplified feedback linearization control of a three-phase PV inverter with an LCL filter has been proposed by Bao et al. [54]. Their work aims to increase the decoupling performance of the control system, and improve its dynamic performance and adaptability. An integrated design approach for LCL filters based on nonlinear inductors for grid-connected inverter applications has been proposed by Sgrò et al. [55]. Their work present a modified design procedure for an LCL filter topology that takes into account the optimization of the current control loop in terms of robustness and dynamic performance. Based on the analysis of equations describing the behavior of the filter, a new methodology integrating the design of the filter inductances, a predictive controller and an active damping method have been developed. Li et al. have proposed an improved proportional resonant (PR) control strategy for a three-phase grid-connected inverter with LCL filter based on active damping [56]. In this work, the authors first compared and analyzed the proportional resonance technique and the quasiproportional resonance to the improved PR controller. In the second stage, the improved PR controller is compared with the traditional controller of the three-phase grid-connected inverter with LCL filter based on active damping. The proposed improved current control strategy has good dynamic response. It can realize the current nonstatic error control of the grid-connected, as well as the decoupling control of active and reactive power when the load jumps. In addition, an adaptive harmonic compensation technique with a proportional resonance (PR) and PR integral (PRI) controller is proposed to minimize low-order harmonics [16].

From the above, first-, second-, and third-order passive filters are regularly used in various control strategies of the grid-connected photovoltaic systems in order to reduce the total harmonic distortion (THD) of the current injected into the grid. However, as it can be seen in the literature cited above, the backstepping control strategy has already been applied to control the inverters of the grid-connected photovoltaic systems only for the L and LC filters. However, the first-order filter has the disadvantage of a fairly large voltage drop across its terminals and a high weight in terms of size [57]. Nevertheless, the LCL filter draws more attention from researchers due to its superior performance.

Compared to the first- or second-order filter, it offers significant attenuation of the high-frequency components of harmonic distortions on the one hand, and cost savings in terms of reduced overall weight and component size on the other [58]. LCL filters are also used in grid-connected PV systems to get rid of interactive resonances [59]. In addition, the dynamic model of the LCL filter in the dq synchronous reference frame is nonlinear, high order (6th order), complex, and its implementation through conventional control techniques is very difficult and inaccurate.

1.4. Scopes and Motivation. In view of the aforementioned literature, there is a need for an efficient control technique able to control dynamic systems with high-order variable parameters. Significant attention has recently given to the backstepping approach as one of the most effective approaches to control such systems. The backstepping control technique is a recursive design procedure developed for designing stabilizing controls for a special class of nonlinear dynamical systems built from subsystems. It designing procedure links the choice of a control Lyapunov function with the design of a feedback controller and guarantees global asymptotic stability of strict feedback systems [60]. This control method has two main advantages. On one hand, it has the ability to decompose a complex high-order system into several subsystems of first order and on the other hand, for simplifying the control design procedure, it introduces virtual control signals in each subsystem [61].

1.5. Contributions. The main contribution of this work is to systematically control a high-order differential equation system of a three-phase grid-connected solar photovoltaic system with a LCL output filter (third-order filter) operating under fast sunlight conditions. This is done by using the ability of the backstepping control technique to stabilize at each step any nonlinear dynamic subsystems of first-order leading to the overall stability of the system [8].

This control scheme will contribute

(i) to improve the power quality of the grid-connected solar photovoltaic system operating in the variable and low irradiance conditions by injecting into the grid the highest possible sinusoidal waveform that minimizes the rate of harmonic distortion

(ii) to improve the overall stability of the solar photovoltaic system in closed loop

(iii) to improve the robustness of the system under variable and low irradiance conditions

Thus, this paper deals with the control of a two-level voltage inverter using a nonlinear backstepping controller intended for a three-phase grid-connected photovoltaic system. The proposed backstepping controller uses the nonlinear dynamic model of an LCL filter in the dq synchronous reference frame to generate the reference voltage (Vref) of the two-level voltage inverter. The main rule of this control technique is the reactive power compensation and the reduction of the harmonic distortions generated by the inverter.

1.6. Organization of the Paper. The rest of the research article is structured as follows in the next sections. Section 2 concern the description and modeling of a grid-connected PV system. This section ends with the design of the nonlinear backstepping controller. Numerical simulations are used in Section 3 to illustrate the effectiveness of the controller in minimizing the harmonic distortions rate and improving the power factor of the grid-connected PV system. The article ends with a conclusion in Section 4.

2. Materials and Methods

2.1. Description of the Grid-Connected Photovoltaic System. The three-phase two-stage grid-connected solar photovoltaic system that is presented in this article is adapted from the work in [15, 62, 63]. Its general diagram which consists of five groups of blocks is presented in Figure 1. The first block group is composed of a photovoltaic power source (PV block) connected to a voltage step-up chopper (DC-DC block). This first group of blocks also contains a maximum power point tracking controller (MPPT block) associated with a PI regulator (PI block), making it possible to improve the performance of the PV block via the DC-DC block. The second block comprises a capacitor C_{dc} used to filter the supply voltage of the two-level inverter (DC-AC block). The inverter is driven by a vector pulse width modulation signal (SVPWM block) and then injects into the grid a three-phase alternating current. The third group is made up of a third-order filter which filters the harmonic distortions of the current injected into the grid by the inverter of the PV system. The fourth group contains a nonlinear load composed of a graëtz bridge (AC-DC block) supplying a load (P2, Q2) and a linear load (P1, Q1) connected to the network. The fifth group consists only of the block describing the proposed backstepping technique.

2.2. Mathematical Modeling of PV Systems. According to Kirchhoff's law relating to currents applied to the electrical circuit of Figure 1, the following relationship is obtained:

$$C_{dc}\frac{dV_{dc}}{dt} = i_{out} - i_{dc}, \tag{1}$$

where V_{dc} is the voltage across the filter capacitor C_{dc}. i_{out} and i_{dc} are, respectively, DC-DC boost converter output current and inverter input current.

According to the law of conservation of energy and neglecting the power losses of the inverter, the power balance relationship between DC side, i.e., the input of the inverter and AC side of the inverter, i.e., the output can be given by the following relationship [64, 65]:

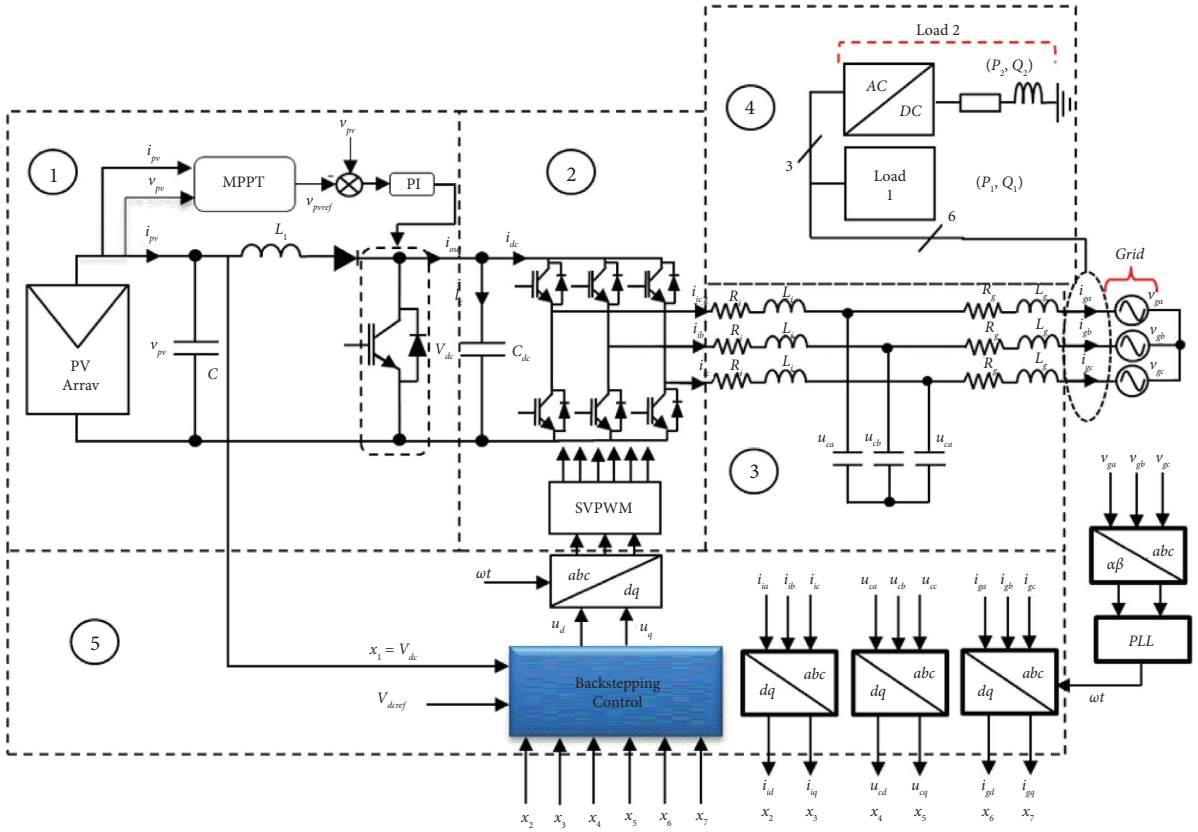

Figure 1: Grid-connected photovoltaic system.

$$\begin{aligned} P_{\mathrm{dc}} &= P_{\mathrm{ac}} \\ &= V_{\mathrm{dc}} i_{\mathrm{out}} \\ &= \frac{3}{2}\left(v_{\mathrm{gd}} i_{\mathrm{gd}} + v_{\mathrm{gq}} i_{\mathrm{gq}}\right), \end{aligned} \tag{2}$$

where v_{gd}, v_{gq}, i_{gd}, and i_{gq} are, respectively, the grid voltages and currents in the dq synchronous reference frame. The average value of v_{gq} is equal to zero in steady state. Then, by replacing (2) in (1), the dynamic of the DC link voltage can be expressed as follows:

$$\frac{\mathrm{dV_{dc}}}{\mathrm{dt}} = \frac{3 v_{\mathrm{gd}} i_{\mathrm{gd}}}{2 C_{\mathrm{dc}} V_{\mathrm{dc}}} - \frac{i_{\mathrm{dc}}}{C_{\mathrm{dc}}}. \tag{3}$$

The single-phase model of the LCL filter in the reference frame (*abc*) is represented in Figure 2.

In Figure 2, R_i and L_i are, respectively, the filter resistance and the inductance on the inverter side; R_g and L_g are, respectively, the filter resistance and inductance on the grid side; C_2 and R_d are capacitance and damping resistance of the filter, respectively; ω being the pulsation of the grid.

The mathematical model by phase of the filter in the state space is given by the following equation:

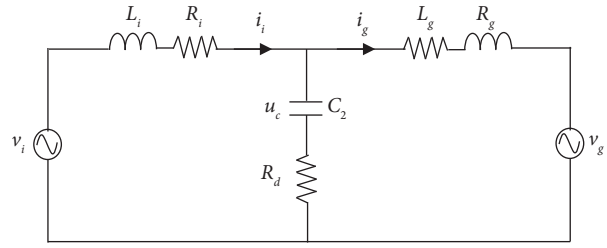

Figure 2: Single-phase LCL filter equivalent circuit.

$$\begin{cases} L_i \dfrac{\mathrm{di}_i}{\mathrm{dt}} = -\left(R_i + R_d\right) i_i + R_d i_g - u_c + v_i, \\ L_g \dfrac{\mathrm{di}_g}{\mathrm{dt}} = -\left(R_i + R_d\right) i_g + R_d i_i + u_c - v_g, \\ C_2 \dfrac{\mathrm{dv}_c}{\mathrm{dt}} = i_i - i_g. \end{cases} \tag{4}$$

In applying the Park transform to the system of equation (4), the dynamic mathematical model of the LCL filter in Park's dq synchronous rotating frame can be described as follows:

$$\begin{cases} \dfrac{\mathrm{di_{gd}}}{\mathrm{dt}} = -\dfrac{R_g}{L_g} i_{\mathrm{gd}} + \dfrac{1}{L_g} u_{\mathrm{cd}} + \omega i_{\mathrm{gq}} - \dfrac{1}{L_g} v_{\mathrm{gd}}, \\ \dfrac{\mathrm{di_{gq}}}{\mathrm{dt}} = -\dfrac{R_g}{L_g} i_{\mathrm{gq}} + \dfrac{1}{L_g} u_{\mathrm{cq}} - \omega i_{\mathrm{gd}} - \dfrac{1}{L_g} v_{\mathrm{gq}}, \\ \dfrac{\mathrm{du_{cd}}}{\mathrm{dt}} = \dfrac{1}{C}\left(i_{\mathrm{id}} - i_{\mathrm{gd}}\right) + \omega u_{\mathrm{cq}}, \\ \dfrac{\mathrm{du_{cq}}}{\mathrm{dt}} = \dfrac{1}{C}\left(i_{\mathrm{iq}} - i_{\mathrm{gq}}\right) - \omega u_{\mathrm{cd}}, \\ \dfrac{\mathrm{di_{id}}}{\mathrm{dt}} = -\dfrac{R_i}{L_i} i_{\mathrm{id}} - \dfrac{1}{L_i} u_{\mathrm{cd}} + \omega i_{\mathrm{iq}} + \dfrac{1}{L_i} v_i, \\ \dfrac{\mathrm{di_{iq}}}{\mathrm{dt}} = -\dfrac{R_i}{L_i} i_{\mathrm{iq}} - \dfrac{1}{L_i} u_{\mathrm{cq}} - \omega i_{\mathrm{id}} + \dfrac{1}{L_i} v_{\mathrm{iq}}, \end{cases} \tag{5}$$

where

$$\begin{cases} x_1 = V_{\mathrm{dc}}; x_2 = i_{\mathrm{gd}}; x_3 = i_{\mathrm{gq}}; x_4 = u_{\mathrm{cd}}; x_5 = u_{\mathrm{cq}}; x_6 = i_{\mathrm{id}}; x_7 = i_{\mathrm{iq}}, \\ a_1 = \dfrac{R_i}{L_i}; a_2 = \dfrac{R_g}{L_g}, \\ \delta_1 = \dfrac{1}{L_i}; \delta_2 = \dfrac{1}{L_g}; \delta_3 = \dfrac{1}{C}; \delta_4 = \dfrac{1}{C_{\mathrm{dc}}}. \end{cases} \tag{6}$$

By substituting equations (3) in (5), the grid-connected photovoltaic system can be described by the final dynamic mathematical model of the LCL filter as follows:

$$\begin{cases} \dot{x}_1 = \dfrac{3\delta_4 v_{\mathrm{gd}}}{2x_1} x_2 - \delta_4 i_{\mathrm{dc}}, \\ \dot{x}_2 = -a_2 x_2 + \delta_2 x_4 + \omega x_3 - \delta_2 v_{\mathrm{gd}}, \\ \dot{x}_3 = -a_2 x_3 + \delta_2 x_5 - \omega x_2 - \delta_2 v_{\mathrm{gq}}, \\ \dot{x}_4 = \delta_3\left(x_6 - x_2\right) + \omega x_5, \\ \dot{x}_5 = \delta_3\left(x_7 - x_3\right) - \omega x_4, \\ \dot{x}_6 = -a_1 x_6 - \delta_1 x_4 + \omega x_7 + \delta_1 v_{\mathrm{id}}, \\ \dot{x}_7 = -a_1 x_7 - \delta_1 x_5 - \omega x_6 + \delta_1 v_{\mathrm{iq}}. \end{cases} \tag{7}$$

2.3. Backstepping Control Design. This section is devoted to the development of a backstepping controller for grid-connected inverters with LCL-type third-order filters at the output. The dynamic system of equations in equation (7) is of order seven and has seven state vectors. The design of the regulator will also be done in seven steps.

Step 1. Stabilization of the first subsystem (first equation)

Considering the following first subsystem to be stabilized,

$$\dot{x}_1 = \frac{3\delta_4 v_{\mathrm{gd}}}{2x_1} x_2 - \delta_4 i_{\mathrm{dc}}. \tag{8}$$

The first regulation error between the measurement $x_1 = V_{\mathrm{dc}}$ and its reference $x_{1d} = V_{\mathrm{dcref}}$ is

$$z_1 = x_1 - x_{1d}. \tag{9}$$

The derivative of the regulation error becomes

$$\dot{z}_1 = \dot{x}_1 - \dot{x}_{1d} = \frac{3\delta_4 v_{\mathrm{gd}}}{2x_1} x_2 - \delta_4 i_{\mathrm{dc}} - \dot{x}_{1d}. \tag{10}$$

In this first subsystem, $x_2 = i_{gd}$ is considered as a virtual command. If α_2 is the form that x_2 must have to stabilize the first subsystem, then the regulation error will be

$$z_2 = x_2 - \alpha_2. \tag{11}$$

Substituting $x_2 = z_2 + \alpha_2$ in the derivative (10) gives

$$\dot{z}_1 = \frac{3\delta_4 v_{gd}}{2x_1}(z_2 + \alpha_2)x_2 - \delta_4 i_{dc} - \dot{x}_{1d}. \tag{12}$$

Let us choose a Lyapunov function V_1 in quadratic form, in order to determine the first virtual command α_2 so that

$$V_1 = \frac{1}{2}z_1^2. \tag{13}$$

Its derivative becomes

$$\dot{V}_1 = z_1\dot{z}_1 = \frac{3\delta_4 v_{gd}}{2x_1}z_1z_2 + z_1\left(\frac{3\delta_4 v_{gd}}{2x_1}\alpha_2 - \delta_4 i_{dc} - \dot{x}_{1d}\right). \tag{14}$$

To determine the virtual command α_2 which ensures the negativity of the derivative $\dot{V}_1$ of the Lyapunov function V_1, the following equality is stated from equation (14):

$$z_1\left(\frac{3\delta_4 v_{gd}}{2x_1}\alpha_2 - \delta_4 i_{dc} - \dot{x}_{1d}\right) = -k_1 z_1^2, \tag{15}$$

where k_1 is a design constant, with $k_1 > 0$.

$$\alpha_2 = \frac{2x_1}{3\delta_4 v_{gd}}\left(-k_1 z_1 + \delta_4 i_{dc} + \dot{x}_{1d}\right). \tag{16}$$

By replacing α_2 from equations (16) in (14), the following derivative of the Lyapunov function $\dot{V}_1$ is obtained:

$$\dot{V}_1 = -k_1 z_1^2 + \frac{3\delta_4 v_{gd}}{2x_1}z_1z_2. \tag{17}$$

From equation (17), it is noted that if $z_2 = 0$, then, $\dot{V}_1 = -k_1 z_1^2 < 0$, which means that $z_1 \longrightarrow 0$. The convergence of z_2 will be obtained at the next step.

Step 2. Stabilization of the second subsystem (2nd equation)

Let the second subsystem be stabilized, and it will be as follows:

$$\dot{x}_2 = -a_2x_2 + \delta_2x_4 + \omega x_3 - \delta_2 v_{gd}. \tag{18}$$

The second regulation error between the measurement $x_2 = i_{gd}$ and its reference $\alpha_2 = i_{gdref}$ which is the virtual control obtained in Step 1:

$$z_2 = x_2 - \alpha_2. \tag{19}$$

The derivative of the regulation error becomes

$$\begin{aligned}\dot{z}_2 &= \dot{x}_2 - \dot{\alpha}_2 \\ &= -a_2x_2 + \delta_2x_4 + \omega x_3 - \delta_2 v_{gd} - \dot{\alpha}_2.\end{aligned} \tag{20}$$

In this second subsystem, x_4 is considered as a virtual command. If α_4 is the form that x_4 must have to stabilize the second subsystem, then the regulation error will be

$$z_4 = x_4 - \alpha_4. \tag{21}$$

Substituting $x_4 = z_4 + \alpha_4$ in the derivative (20) leads to

$$\dot{z}_2 = -a_2x_2 + \delta_2(z_4 + \alpha_4) + \omega x_3 - \delta_2 v_{gd} - \dot{\alpha}_2. \tag{22}$$

Let us choose an extended Lyapunov function V_2, in order to determine the second virtual command α_4 so that

$$V_2 = V_1 + \frac{1}{2}z_2^2. \tag{23}$$

Its derivative becomes

$$\begin{aligned}\dot{V}_2 &= \dot{V}_1 + z_2\dot{z}_2 \\ &= -k_1 z_1^2 + \frac{3\delta_4 v_{gd}}{2x_1}z_1z_2 + z_2\dot{z}_2.\end{aligned} \tag{24}$$

Replacing $\dot{V}_1$ and $\dot{z}_2$, respectively, from equations (20) and (22) into (24) gives

$$\dot{V}_2 = -k_1 z_1^2 + \delta_2 z_2 z_4 + z_2\left(\frac{3\delta_4 v_{gd}}{2x_1}z_1 - a_2x_2 + \delta_2\alpha_4 + \omega x_3 - \delta_2 v_{gd} - \dot{\alpha}_2\right). \tag{25}$$

To determine the virtual command α_4 which ensures the negativity of the derivative $\dot{V}_2$ of the extended Lyapunov function V_2, the following equality is stated from equation (25):

$$z_2\left(\frac{3\delta_4 v_{gd}}{2x_1}z_1 - a_2x_2 + \delta_2\alpha_4 + \omega x_3 - \delta_2 v_{gd} - \dot{\alpha}_2\right) = -k_2 z_2^2, \tag{26}$$

where k_2 is a design constant, with $k_2 > 0$.

$$\alpha_4 = \delta_2^{-1}\left(-k_2 z_2 - \frac{3\delta_4 v_{gd}}{2x_1}z_1 + a_2x_2 - \omega x_3 + \delta_2 v_{gd} + \dot{\alpha}_2\right). \tag{27}$$

By replacing α_4 of equations (27) in (25), the following derivative of the Lyapunov function $\dot{V}_2$ is obtained:

$$\dot{V}_2 = -k_1 z_1^2 - k_2 z_2^2 + \delta_2 z_2 z_4. \tag{28}$$

From equation (28), it is noted that if $z_4 = 0$, then, $\dot{V}_2 = -k_1 z_1^2 - k_2 z_2^2 < 0$, which means that $z_1 \longrightarrow 0$ and $z_2 \longrightarrow 0$. The convergence of z_4 will be obtained in the third step.

By following the same method as in Steps 1 and 2, the third to the seventh subsystems can be successively stabilized. Table 1 gives the Lyapunov function used at each step,

Table 1: Lyapunov function used at each stabilization steps and the obtained virtual commands and the filter input voltages.

Step	Lyapunov function	Virtual commands	Filter input voltage
1	$V_1 = 1/2z_1^2$	$\alpha_2 = 2x_1/3\delta_4 v_{gd}(-k_1 z_1 + \delta_4 i_{dc} + \dot{x}_{1d})$	—
2	$V_2 = V_1 + 1/2z_2^2$	$\alpha_4 = \delta_2^{-1}(-k_2 z_2 - 3\delta_4 v_{gd}/2x_1 z_1 + a_2 x_2 - \omega x_3 + \delta_2 v_{gd} + \dot{\alpha}_2)$	—
3	$V_3 = V_2 + 1/2z_3^2$	$\alpha_5 = \delta_2{}^{-1}(-k_3 z_3 + a_2 x_3 + \omega x_2 + \delta_2 v_{gq} + \dot{x}_{3d})$	—
4	$V_4 = V_3 + 1/2z_4^2$	$\alpha_6 = \delta_3{}^{-1}(-k_4 z_4 - \delta_2 z_2 + \delta_3 x_2 - \omega x_5 + \dot{\alpha}_4)$	—
5	$V_5 = V_4 + 1/2z_5^2$	$\alpha_7 = \delta_3{}^{-1}(-k_5 z_5 - \delta_2 z_3 + \delta_3 x_3 + \omega x_4 + \dot{\alpha}_5)$	—
6	$V_6 = V_5 + 1/2z_6^2$	—	$v_{id} = \delta_1^{-1}(-k_6 z_6 - \delta_3 z_4 + a_1 x_6 + \delta_1 x_4 - \omega x_7 + \dot{\alpha}_6)$
7		—	$v_{iq} = \delta_1^{-1}(-k_7 z_7 - \delta_3 z_5 + a_1 x_7 + \delta_1 x_5 + \omega x_6 + \dot{\alpha}_7)$

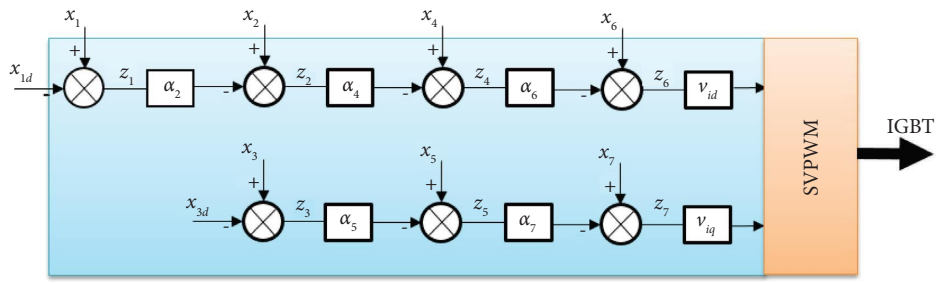

Figure 3: Backstepping controller block diagram.

obtained virtual commands, and the filter input voltages (v_{id}, v_{iq}) in the dq synchronous reference frame. These two components of the filter input voltage are necessary to build the SVPWM needed to drive the electronic switches (IGBT) of the inverter. Constants k_3, k_4, k_5, k_6, and k_7 are design constants defined during the stabilization of the third to the seventh subsystems. The seven steps of the stabilization of the system can be implemented through the block diagram of Figure 3. Abbreviations used in this paper are listed in Table 2.

In Figure 3, $x_{1d} = V_{dcref}$ and $x_{3d} = i_{gqref}$.

3. Results and Discussion

To evaluate the performance of the designed backstepping controller applied to the two-level inverter based on the LCL filter model, numerical simulations were carried out in the MATLAB/Simulink platform using the same test conditions as those of the proportional integral (PI) controller proposed in [66] and synergic control in [15, 63]. The parameters of the PV generator used in this work are listed in Table 3. The overall system is tested and validated with the system parameters listed in Table 4.

To generate drive pulses, the space vector PWM (SVPWM) was used. The initial irradiance value is fixed at 1000 W/m^2; after every 0.5 s, it changes, respectively, to the following values: 500 W/m^2, 750 W/m^2, and 250 W/m^2 to have irradiance variations in a short time and to test the ability of the controller to follow the appropriate value of power generated by the PV generator. These changes in the irradiance are shown in Figure 4. This solar irradiance profile is applied to the photovoltaic array with the aim of simulating the proposed system under different conditions and examining the dynamic response of the backstepping controller. Throughout the simulation, the temperature is maintained at 25°C.

3.1. Grid-Tied Photovoltaic System Performance Indices

3.1.1. Total Power Injected into the Grid. The total power injected into the electrical grid for 2 s according to the solar irradiance profile of Figure 4 is shown in Figure 5. At $t = 0$ s, when the solar irradiance is 1000 W/m^2, the instantaneous active power in steady state is approximately 100 kW after a response time tr = 15.05 ms. Moreover, at $t = 0.5$ s, the solar irradiance is 500 W/m^2, slight oscillations are observed during the transient phase which lasts about tr = 19.82 ms. The instantaneous active power in steady state is approximately 50.57 kW at this solar irradiance. At $t = 1$ s, the solar irradiance passes at 750 W/m^2. The oscillations decrease more during the transient phase which lasts tr = 28.5 ms, and the instantaneous active power in the steady state is about 75.57 kW. Finally, at $t = 1.5$ s, the solar irradiance passes at 250 W/m^2. The oscillations increase further during a response time of 15.36 ms. Then the instantaneous active power in steady state is around 25.56 kW at this solar irradiance. Thus, it can be seen that the active power injected into the grid by the PV system is the maximum one expected at each irradiance value. So, the proposed control scheme allows to extract the maximum power from the PV panels.

3.1.2. Reactive Power. The total reactive power injected or transmitted into the electrical grid for 2 s according to the solar irradiance profile of Figure 4 is illustrated in Figure 6. It can be seen that this power is almost constant over time. In other words, the reactive power transmitted by the PV system is very low and oscillates around almost zero constantly over time regardless of the irradiance value.

3.1.3. Power Factor. The power factor of the studied grid-connected photovoltaic system for the given irradiance profile is illustrated in Figure 7. It is equal to 0.988 during the

Table 2: Acronyms and parameters used in this paper.

PV	Photovoltaic
PI	Proportional-integral controller
PID	Proportional-integral-derivative controller
THD	Total harmonics distortion
MPPT	Maximum power point tracking
DC/AC	Direct current/Alternating current
SMC	Sliding mode control
ZN	Ziegler–Nichols
PSO	Particle swarm optimization
PLL	Phase-locked loop
DPC	Direct power controller
SVPWM	Vector pulse width modulation
i_{pv}	Photovoltaic array current (A)
v_{pv}	Photovoltaic array voltage (V)
V_{pvref}	Reference photovoltaic array voltage (V)
L_1	Boost converter current smoothing inductance (A)
C	Boost converter parasitic filtering capacity (μF)
R_c	Internal resistance of the parasitic filtering capacity of the boost converter (Ω)
C_{dc}	Inverter filtering capacity (μF)
V_{dc}	DC link voltage (V)
V_{dcref}	Reference DC link voltage (V)
i_{out}	Boost converter output current (A)
i_{dc}	Inverter input current (A)
C_2	Capacitance of the filter (μF)
R_d	Damping resistance of the filter (Ω)
P_{dc}	Power available at DC side of the inverter (W)
P_{ac}	Power available at AC side of the inverter (W)
i_c	Inverter filtering capacity current (A)
i_{ia}, i_{ib}, i_{ic}	Inverter rated current (A)
i_{id}, i_{iq}	dq inverter rated current (A)
L_i, R_i	Filter inductance (H) and resistance (Ω) on the inverter side
u_{ca}, u_{cb}, u_{cc}	Voltages across the filter capacitors (V)
u_{cd}, u_{cq}	dq voltages across the filter capacitors (V)
L_g, R_g	Mains side filter inductance (H) and resistance (Ω)
i_{ga}, i_{gb}, i_{gc}	Currents injected into the ac grid (A)
i_{gd}, i_{gq}	Grid currents in the dq synchronous reference frame (V)
v_{ga}, v_{gb}, v_{gc}	Voltages at the ac grid side (V)
v_{gd}, v_{gq}	Grid voltages in the dq synchronous reference frame (V)

Table 2: Continued.

V_i, $i = 1 to 6$	Lyapunov function used from step 1 to step 6 of the backstepping control scheme (V)
ω	Pulsation of the grid (rad/s)
$x_1 = V_{dc}$; $x_2 = i_{gd}$; $x_3 = i_{gq}$; $x_4 = u_{cd}$; $x_5 = u_{cq}$; $x_6 = i_{id}$; $x_7 = i_{iq}$	Components of state vector of the system
δ_i, $i = 1 to 4$	Constant
x_{1d}, x_{3d}	Components of the system reference state vector
$\alpha_2, \alpha_4, \alpha_5, \alpha_6, \alpha_7$	Virtual command
z_i, $i = 1 to 7$	Regulation error
k_i, $i = 1 to 7$	Design constant
v_{id}, v_{iq}	Final control law on the direct and quadratic axis
i_i, i_g	Current on the inverter side and on the grid side

Table 3: PV generator parameters.

Number of cell	96	I_{sC}	5.96 A
N_p	66	V_{0C}	64.2 V
N_s	5	V_{mp}	54.7 V
R_s	0.037 Ω	R_p	993.51 Ω
P	305 W	Total power	126.26 kW

Table 4: Power system parameters.

L_1	$3.2.10^{-6}$ H	L_g	500.10^{-6} H	k_7	35.10^7
C	100.10^{-6} F	R_i	20.10^{-3} Ω	f	50 Hz
C_{dc}	$3500\,\mu_F$	R_g	20.10^{-3} Ω	f_{sw}	25 kHz
V^*_{dc}	$600\,V$	k_1	8300	T	25℃
P_1	95 kW	k_2	16.10^3	Sample time	10^{-6} s
P_2	5 kW	k_3	16.10^3	Switch on	0.65 – 0.75 s
Q_1	2 kVar	k_4	22.10^5		
Q_2	1 kVar	k_5	22.10^5		
L_i	500.10^{-6} H	k_6	35.10^7		

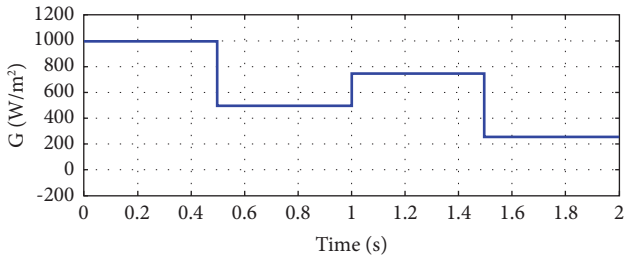

Figure 4: Solar irradiance profile applied to the photovoltaic generator.

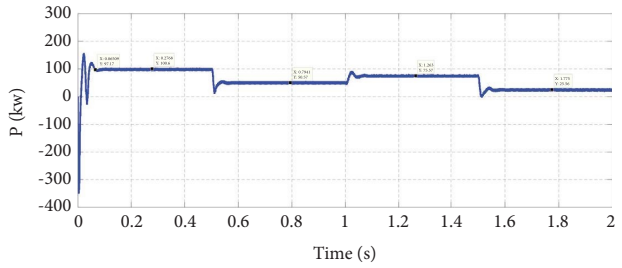

Figure 5: Active power injected to the grid by the PV system according to variations in irradiance.

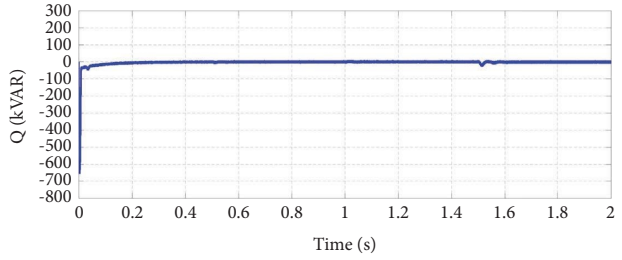

Figure 6: Reactive power transmitted into the grid by the PV system according to variations in irradiance.

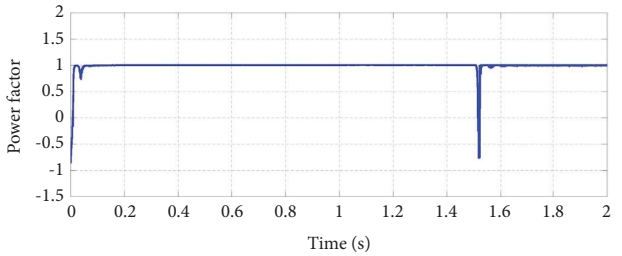

Figure 7: Power factor according to variations in irradiance.

entire period of time when the solar irradiance varies; proving that the reactive power is almost zero. It is nevertheless observed a large and rapid drop in the power factor at $t = 1.5$ s when the solar irradiance drops from 750 W/m^2 to 250 W/m^2.

3.2. DC Bus Voltage. The DC bus voltage V_{dc} (curve in red) and its reference (curve in blue) $V_{dcref} = 600$ V are illustrated in Figure 8. At $t = 0$ s, the solar irradiance $G = 1000$ W/m^2 is applied to the photovoltaic generator, a response time tr = 22.32 ms is observed during the transient phase, after which the DC bus voltage returns to its reference value of 600 V in steady state. Moreover, at $t = 0.5$ s, the solar irradiance $G = 500$ W/m^2 is applied to the photovoltaic generator, a response time tr = 8.6 ms is observed during the transient phase, after which the DC bus voltage returns to the reference value of 600 V in steady state. At $t = 1$ s, the solar irradiance increases to the value $G = 750$ W/m^2, a response time tr = 29 ms is observed during the transient phase, after which the DC bus voltage returns to its reference value in the steady state. Finally, at $t = 1.5$ s, the solar irradiance decreases to the value $G = 250$ W/m^2, a response time tr = 26.05 ms is observed during the transient phase, after which the DC bus voltage also returns to its reference value

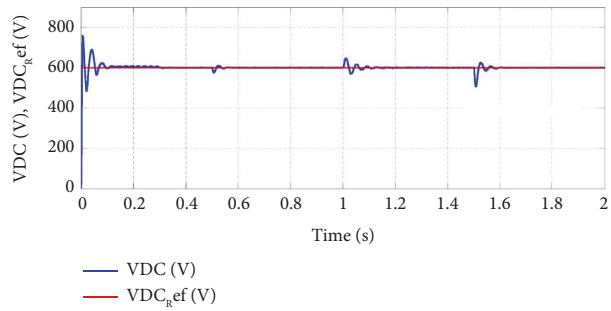

Figure 8: DC bus voltage according to variations in irradiance.

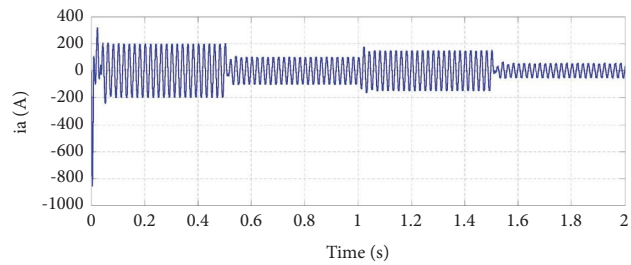

Figure 9: Instantaneous current in phase number *a* of the grid according to the variation in irradiance.

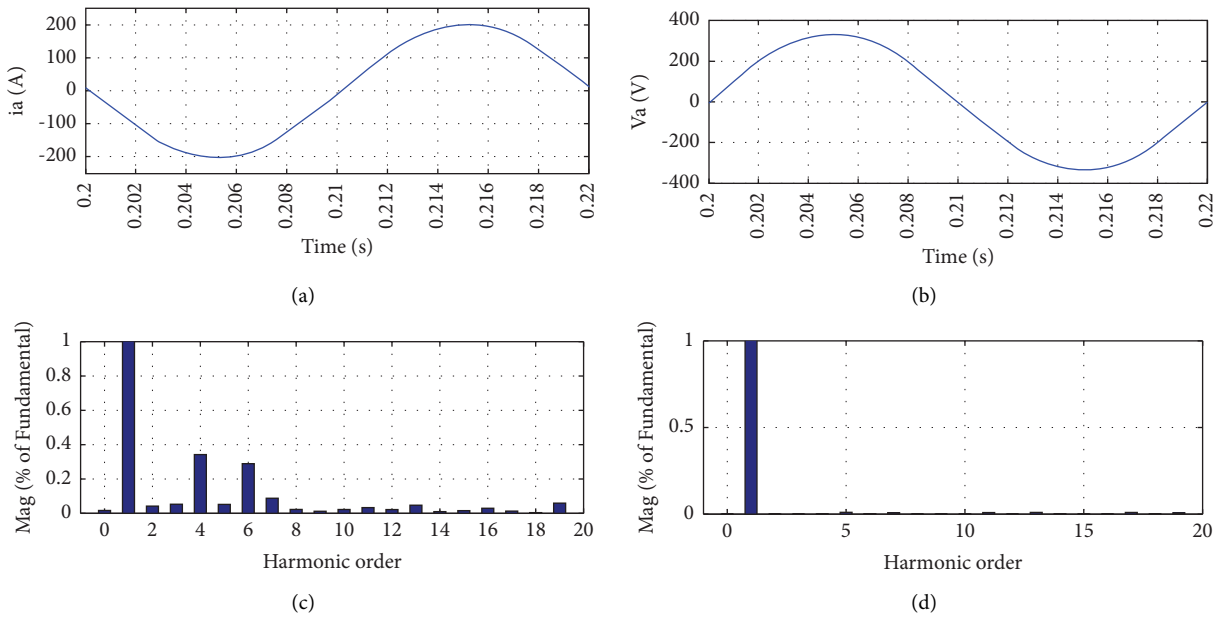

Figure 10: Zooms of current (a) and voltage (b) of phase number *a* and their harmonic spectrum at 1000 W/m^2. (c) Harmonic spectrum of current (Fundamental (50 Hz) = 200.7, THD = 0.48%). (d) Harmonic spectrum of voltage (Fundamental (50 Hz) = 326.6, THD = 0.24%).

in the steady state. Thus, it is noted that the DC bus voltage perfectly follows its set point value whatever the value of the irradiance is.

3.3. Instantaneous Current in the Grid. The instantaneous current of phase *a* during the variation of the irradiance is presented in Figure 9. At $t = 0$ s, the solar irradiance applied to the photovoltaic generator is $G = 1000$ W/m^2, the maximum intensity of the current injected into the grid is about 200 A. At $t = 0.5$ s, the solar irradiance applied to the photovoltaic generator is $G = 500$ W/m^2, the grid receives a current with a maximum intensity of about 100 A. At $t = 1$ s, the solar irradiance applied to the photovoltaic generator is $G = 750$ W/m^2, the instantaneous current in the grid has a maximum value of about 149 A. Finally, at $t = 1.5$ s, the solar irradiance applied to the photovoltaic generator is

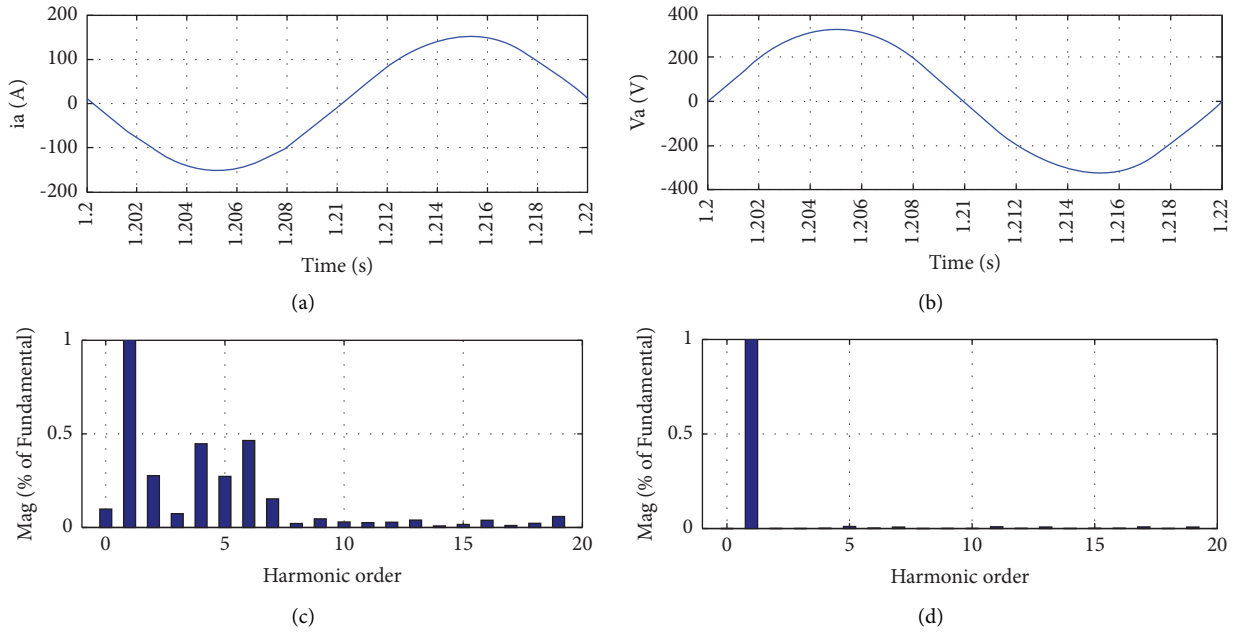

FIGURE 11: Zooms of current (a) and voltage (b) of phase number *a* and their harmonic spectrum at 750 W/m^2. (c) Harmonic spectrum of current (Fundamental (50 Hz) = 150.5, THD = 0.78%). (d) Harmonic spectrum of voltage (Fundamental (50 Hz) = 326.6, THD = 0.41%).

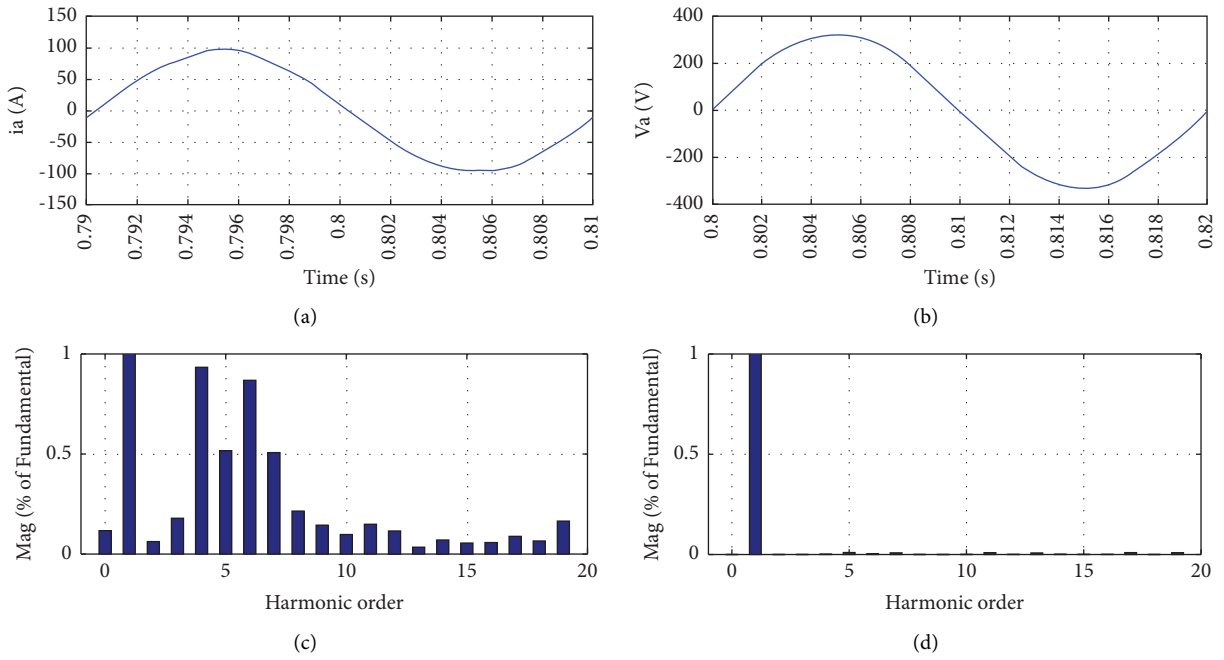

FIGURE 12: Zooms of current (a) and voltage (b) of phase number *a* and their harmonic spectrum at 500 W/m^2. (c) Harmonic spectrum of current (Fundamental (50 Hz) = 95.32, THD = 1.22%). (d) Harmonic spectrum of voltage (Fundamental (50 Hz) = 326.6, THD = 0.46%).

$G = 250$ W/m^2 and the maximum intensity of the current injected into the grid is about 56 A. Globally, the maximum value of the current in that phase is proportional to the irradiance value. This is directly linked to the behavior of the current provided by the PV modules.

3.4. Zooms of Voltage, Current, and Harmonic Spectra Injected into the Grid for Different Irradiances. Figures 10–13 show the zooms of current and voltage of phase number *a*, as well as their respective harmonic spectra for different irradiance values.

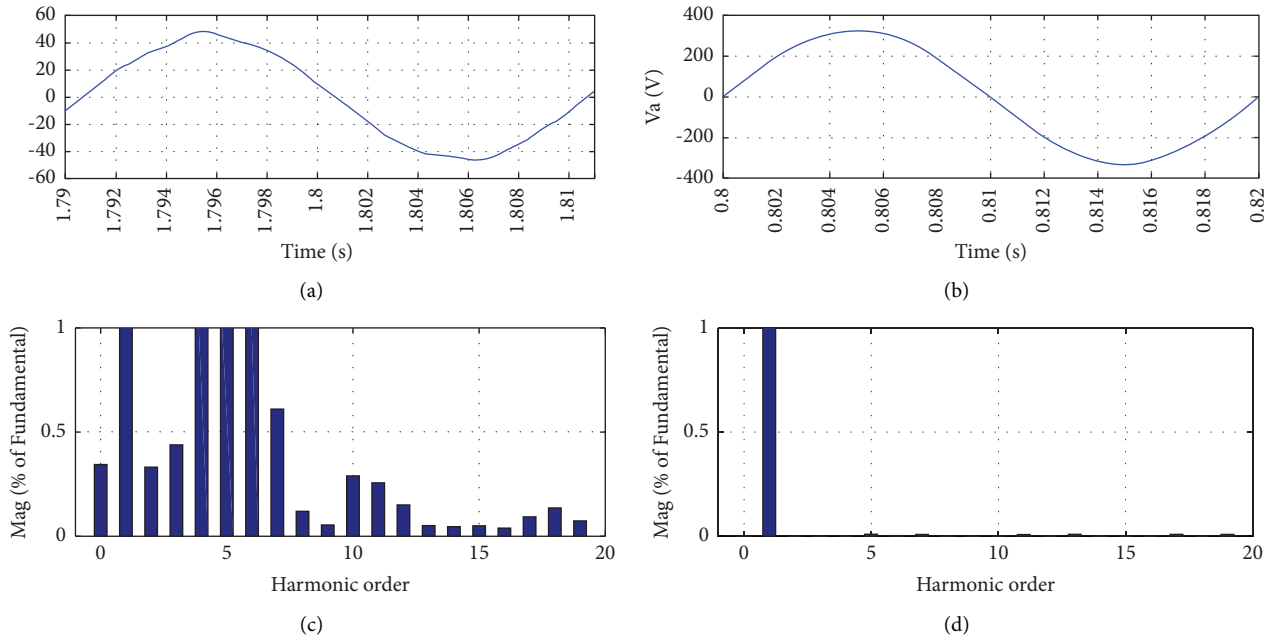

Figure 13: Zooms of current (a) and voltage (b) of phase number a and their harmonic spectrum at 250 W/m^2. (c) Harmonic spectrum of current (Fundamental (50 Hz) = 44.15, THD = 2.16%). (d) Harmonic spectrum of voltage (Fundamental (50 Hz) = 326.6, THD = 0.51%).

Table 5: Comparative table of THD$_{i_a}$ (%) for different solar irradiance levels.

Reference	Algorithm type	G (W/m^2)			
		1000	750	500	250
		THDia (%)			
Nguyen [66]	PI	1.41	1.82	1.93	3.83
Qian et al. [63]	Synergetic control	1.13	1.27	1.81	3.46
Pesdjock et al. [15]	Improved synergetic control	1.02	1.10	1.25	2.32
Wai et al. [23]	Backstepping control with LC filter	1.29	—	—	—
Diouri et al. [8]	Backstepping control with LC filter	0.78	—	—	—
Xu et al. [64]	Backstepping control	1.62	—	—	—
Xu et al. [64]	Adaptive fuzzy sliding mode command-filtered backstepping (AFSCB)	0.53	—	—	—
Roy and Mahmud [65]	Nonlinear robust adaptive	2.12	—	—	—
Roy and Mahmud [65]	Backstepping controller (NRABC)	2.20	—	—	—
Roy et al. [50]	Nonlinear backstepping control	3.20	—	—	—
Our study	Backstepping control with LCL filter	0.5	0.8	1.15	2.09

Table 6: Efficiency of inverter under different solar irradiation values.

Control strategy	Solar irradiance (W/m^2)	Inverter efficiency (%)
This study's backstepping control with LCL filter	1000	97.06
	500	94.94
	750	96.51
	250	95.33

In Figure 10(c), the frequency analysis of the current injected in the grid by the phase number a of the inverter is given when the solar irradiance is 1000 W/m^2. Its fundamental is around 232.1 A at a frequency of 50 Hz, and the current THD is about 0.48%. Figure 11(c) presents the same frequency analysis when the solar irradiance is 750 W/m^2. The fundamental is around 169.9 A at 50 Hz, and the THD is about 0.78%. Figure 12(c) shows the frequency analysis when the solar irradiance is 500 W/m^2. The fundamental is around 107.6 A at 50 Hz, and the THD is around 1.22%. Finally, Figure 13(c) shows the frequency analysis when the solar irradiance is 250 W/m^2. Its fundamental is about 47.19 A at 50 Hz, and the THD is about 2.16%. This leads to the conclusion that the backstepping control based on an LCL filter proposed for the control of the grid-connected inverter in PV system allows to have low current harmonic distortion rates in the grid whatever the solar irradiance. Therefore, a high power quality is obtained in the considered PV power system.

Nevertheless, this power quality degrades as the value of the solar irradiance becomes lower and lower as discussed by Tchoffo Houdji et al. [21]. In the meantime, the frequency analysis of the voltage shown in Figures 10(d)–13(d) presents a fundamental of 565.6 V at a frequency of 50 Hz and voltage THD of 0.24%, 0.41%, 0.46%, and 0.51%, respectively, for irradiance values of 1000 W/m^2, 750 W/m^2, 500 W/m^2, and 250 W/m^2. These values of the voltage THD are less that those obtained in the literature with other backstepping controllers for grid-connected inverter (1.90% [23]) and for inverter in standalone PV system (0.78% [8]), proving that the output voltage of the studied grid-connected inverter supplied by the PV system is lightly affected by harmonic distortions.

To highlight the interest of this work, a comparison of the performances of the proposed backstepping controller based on a LCL filter during the variation of the solar irradiance with those in the literature was also carried out. The average values of the current THD collected during various operating tests are presented in Table 5. The efficiency of the inverter operating with the proposed backstepping controller was evaluated for different values of solar irradiance and given in Table 6. Analysis of the results in these tables shows that the THD values obtained with the proposed backstepping controller are always within the accepted standards whatever the solar irradiance variations are. These quantitative and qualitative results show that the proposed control approach has better performance in terms of reducing harmonic distortions of the currents compared to other approaches in the literature [15, 63, 66] and even in terms of efficiency.

4. Conclusion

In this work, a control strategy that could efficiently control a three-phase two-level grid-connected inverter of a photovoltaic system was developed, with the aim of improving the power quality of the electrical grid. Two of the most important constraints of this inverter control system were taken into account, namely, (i) the nonlinearity of the dynamics of the system, and (ii) the high dimension of the system model. For these reasons, a nonlinear controller was proposed. It basically consists of the control law synthesized using the backstepping technique. A theoretical analysis, using Lyapunov's stability theory at each stage of the technique, proves the overall stability of the system. The results of the simulation show that the total harmonic distortion rates of the current are 0.48%, 0.78%, 1.22%, and 2.16%, respectively, for solar irradiance of 1000 W/m^2, 750 W/m^2, 500 W/m^2, and 250 W/m^2; the DC bus voltage is maintained at 600 V, and the power factor is 0.988 for the same irradiance values. Thus, the proposed controller meets its main control objective which was to improve the quality of energy. The simulation results further underline the robustness of the controller with regards to rapid changes in solar irradiance. An experimental study of the proposed backstepping command and an analysis of the cost savings would be done later.

Data Availability

The data used in this article come from simulation of the studied system with the proposed control techniques and carried out in the MATLAB/Simulink platform. These simulation data are available from the corresponding author upon request.

Disclosure

Each author certified that this material or similar material has not been and will not be submitted to or published in any other publication.

Conflicts of Interest

The authors declare that they have no conflicts of interest.

Authors' Contributions

All people who met authorship criteria are listed as authors, and all the authors have certified that they have participated sufficiently in the work to take public responsibility for the content, including participation in the concept, design, analysis, writing, or revision of the manuscript. Specifically, I. F. Bendé, E. Tchoffo Houdji, and J. L. Nsouandélé conceived the present idea. I. F. Bendé, E. Tchoffo Houdji, and G. B. Tchaya developed the theory and performed the computations. J. L. Nsouandélé, M. Kamta, and Haman-Djalo verified the analytical methods and supervised the findings of this work. I. F. Bendé and E. Tchoffo Houdji wrote the manuscript with support from G. B. Tchaya and J. L. Nsouandélé. All authors discussed the results and contributed to the final manuscript.

References

[1] R. K. Pachauri and A. Reisinger, *Bilan 2007 des changements climatiques: Rapport de synthèse*, Groupe d'experts intergouvernemental sur l'évolution du climat (GIEC), Chennai, India, 2008.

[2] R. Giec and A. R. Pachauri, "Changements climatiques 2014: rapport de synthèse," *Contribution des Groupes de Travail I, II et III au Cinquième Rapport D'évaluation du Groupe d'Experts Intergouvernemental sur l'Évolution du Climat*, GIEC, Genève, Switzerland, 2014.

[3] K. Ali, L. Khan, Q. Khan et al., "Robust integral backstepping based nonlinear mppt control for a pv system," *Energies*, vol. 12, no. 16, p. 3180, 2019.

[4] H. Doubabi, I. Salhi, M. Chennani, and N. Essounbouli, "High Performance MPPT based on TS Fuzzy–integral backstepping control for PV system under rapid varying irradiance—experimental validation," *ISA Transactions*, vol. 118, pp. 247–259, 2021.

[5] K. Dahech, M. Allouche, T. Damak, and F. Tadeo, "Backstepping sliding mode control for maximum power point tracking of a photovoltaic system," *Electric Power Systems Research*, vol. 143, pp. 182–188, 2017.

[6] A. I. Ali, M. A. Sayed, and E. E. Mohamed, "Modified efficient perturb and observe maximum power point tracking

technique for grid-tied PV system," *International Journal of Electrical Power & Energy Systems*, vol. 99, pp. 192–202, 2018.

[7] K. Ali, Q. Khan, S. Ullah, I. Khan, and L. Khan, "Nonlinear robust integral backstepping based MPPT control for standalone photovoltaic system," *PLoS One*, vol. 15, no. 5, Article ID e0231749, 2020.

[8] O. Diouri, N. Es-Sbai, F. Errahimi, A. Gaga, and C. Alaoui, "Modeling and design of single-phase PV inverter with MPPT algorithm applied to the boost converter using back-stepping control in standalone mode," *International Journal of Photoenergy*, vol. 2019, Article ID 7021578, 16 pages, 2019.

[9] M. Morey, N. Gupta, M. M. Garg, and A. Kumar, "Performance analysis of voltage sensorless based controller for two-stage grid-connected solar PV system," *International Journal of Power Electronics and Drive Systems*, vol. 14, no. 1, pp. 444–452, 2023.

[10] W. Charfi, M. Chaabane, H. Mhiri, and P. Bournot, "Performance evaluation of a solar photovoltaic system," *Energy Reports*, vol. 4, pp. 400–406, 2018.

[11] F. Meng, Q. Zou, Z. Zhang et al., "An intelligent hybrid wavelet-adversarial deep model for accurate prediction of solar power generation," *Energy Reports*, vol. 7, pp. 2155–2164, 2021.

[12] M. Atmaca and İ. Z. Pektemir, "Photovoltaic-thermal system for building application: a case study," *Energy Sources A*, vol. 12, pp. 1–18, 2020.

[13] F. Spertino and G. Graditi, "Power conditioning units in grid-connected photovoltaic systems: a comparison with different technologies and wide range of power ratings," *Solar Energy*, vol. 108, pp. 219–229, 2014.

[14] R. P. Narasipuram, C. Somu, R. T. Yadlapalli, and L. S. Simhadri, "Efficiency analysis of maximum power point tracking techniques for photovoltaic systems under variable conditions," *International Journal of Innovative Computing and Applications*, vol. 9, no. 4, pp. 230–240, 2018.

[15] M. J. P. Pesdjock, J. R. M. Pone, G. Kenne, and L. L. Sonfack, "Contribution of synergetic control to the minimization of harmonics currents injected for grid connected photovoltaic systems," *SN Applied Sciences*, vol. 2, no. 8, pp. 1–8, 2020.

[16] M. Morey, N. Gupta, M. M. Garg, and A. Kumar, "A comprehensive review of grid connected solar photovoltaic system: architecture, control, and ancillary services," *Renewable Energy Focus*, vol. 45, pp. 307–330, 2023.

[17] B. Eristi and H. Eristi, "Classification of power quality disturbances in solar PV integrated power system based on a hybrid deep learning approach," *International Transactions on Electrical Energy Systems*, vol. 2022, Article ID 8519379, 13 pages, 2022.

[18] F. Justin, G. Peter, A. A. Stonier, and V. Ganji, "Power quality improvement for vehicle-to-grid and grid-to-vehicle technology in a microgrid," *International Transactions on Electrical Energy Systems*, vol. 2022, Article ID 2409188, 17 pages, 2022.

[19] V. Gali, P. K. Jamwal, N. Gupta, and A. Kumar, "Multimode control strategy to improve the power quality and autonomy of PV-Wind-BESS based microgrid using harmonic frequency adaptive observer filter," *Electric Power Systems Research*, vol. 225, Article ID 109786, 2023.

[20] Y. Du, D. D. C. Lu, G. James, and D. J. Cornforth, "Modeling and analysis of current harmonic distortion from grid connected PV inverters under different operating conditions," *Solar Energy*, vol. 94, pp. 182–194, 2013.

[21] E. Tchoffo Houdji, D. Yamegueu, and G. B. Tchaya, "Power quality assessment in a stand-alone photovoltaic/battery system supplying an asynchronous motor through an adjustable speed drive," *International Journal of Scientific Engineering and Research*, vol. 10, no. 4, pp. 1157–1167, 2019.

[22] I. D. Bouloumpasis, P. N. Vovos, K. G. Georgakas, and N. A. Vovos, *Harmonic Cancellation of PV-Supplied DC/AC Converter without Stabilizing Input Capacitors*, Elsevier, International Federation of Automatic Control, Amsterdam, Netherlands, 2016.

[23] R. J. Wai, C. Y. Lin, W. Wu, and H. Huang, "Design of backstepping control for high-performance inverter with stand-alone and grid-connected power-supply modes," *IET Power Electronics*, vol. 6, no. 4, pp. 752–762, 2013.

[24] M. Yaïchi, M. Fellah, A. Neçaibia, and A. Mammeri, "Structure of asymmetrical multilevel inverters: application to photovoltaic systems," *International Conference on Energy and Sustainable Development*, vol. 29, pp. 133–143, 2011.

[25] K. Imarazene, H. Chekireb, and E. M. Berkouk, "Selective harmonics elimination pwm with self-balancing dc-link in photovoltaic 7-level inverter," *Turkish Journal of Electrical Engineering and Computer Sciences*, vol. 24, no. 5, pp. 3999–4014, 2016.

[26] A. Mamane, A. Nabil, A. Foulani, and S. Maiga, "Comparative study of linear and non-linear controls of three-phase shunt active filter for improving the quality of electrical energy," *Energy and Power Engineering*, vol. 11, no. 3, pp. 149–166, 2019.

[27] S. K. Sharma and V. Gali, "Development of modified hysteresis current controller switching scheme for multifunctional grid-tied photovoltaic inverters," in *Proceedings of the 2021 1st IEEE International Conference on Power Electronics and Energy (ICPEE)*, pp. 1–6, Bhubaneswar, India, January 2021.

[28] M. Morey, N. Gupta, M. M. Garg, and A. Kumar, "Performance analysis of grid connected SPCS under unbalanced grid voltage, frequency deviation and harmonics," in *Proceedings of the 2022 IEEE PES Innovative Smart Grid Technologies-Asia (ISGT Asia)*, pp. 325–329, Singapore, November 2022.

[29] O. Diouri, F. Errahimi, and N. Es-Sbai, "Regulation of the output voltage of an inverter in case of load variation," *IOP Conference Series: Materials Science and Engineering*, vol. 353, no. 1, pp. 012021–012027, 2018.

[30] Y. Chen and F. Liu, "Design and control for three-phase GridConnected photovoltaic inverter with LCL filter," in *Proceedings of the IEEE Circuits and Systems International Conference on Testing and Diagnosis*, pp. 1–4, Chengdu, China, April 2009.

[31] W. Yin and Y. Ma, "Research on three-phase pv grid-connected inverter based on lcl filter," in *Proceedings of the IEEE 8th Conference on Industrial Electronics and Applications (ICIEA)*, pp. 1279–1283, Melbourne, Australia, June 2013.

[32] N. A. Windarko, O. A. Qudsi, and A. Tjahjono, "Optimized PI constant for current controller of grid connected inverter with LCL filter using Genetic Algorithm," in *Proceedings of the Makassar International Conference on Electrical Engineering and Informatics*, pp. 9–13, Makassar, Indonesia, November 2014.

[33] L. Schirone, F. Celani, and M. Macellari, "Discrete-time control for DC–AC converters based on sliding mode design," *IET Power Electronics*, vol. 5, no. 6, pp. 833–840, 2012.

[34] D.-C. Lee and G.-M. Lee, "Linear control of inverter output voltage in over modulation," *IEEE Transactions on Industrial Electronics*, vol. 44, no. 4, pp. 590–592, 1997.

[35] A. Hasanzadeh, C. S. Edrington, H. Mokhtari, B. Maghsoudlou, and F. Fleming, "Multi-loop linear resonant voltage source inverter controller design for distorted loads using the linear quadratic regulator method," *IET Power Electronics*, vol. 5, no. 6, pp. 841–851, 2012.

[36] I. S. Kim and M. J. Youn, "Variable-structure observer for solar-array current estimation in a photovoltaic power generation system," *IEE Proceedings- Electric Power Applications*, vol. 152, no. 4, pp. 953–959, 2005.

[37] H. Komurcugil, "Steady-state analysis and passivity-based control of single-phase PWM current-source inverters," *IEEE Transactions on Industrial Electronics*, vol. 57, no. 3, pp. 1026–1030, 2010.

[38] R. C. Fanjip, S. R. Dzonde Naoussi, and C. H. Kom, "Fuzzy sliding mode control of a shunt active power filter for harmonic reduction in grid-connected photovoltaic systems," *Journal of Electrical Engineering, Electronics, Control and Computer Science*, vol. 8, no. 27, pp. 43–54, 2022.

[39] M. Lakshmi and S. Hemamalini, "Decoupled control of grid connected photovoltaic system using fractional order controller," *Ain Shams Engineering Journal*, vol. 9, no. 4, pp. 927–937, 2018.

[40] S. Golzari, F. Rashidi, and H. F. Farahani, "A Lyapunov function based model predictive control for three phase grid connected photovoltaic converters," *Solar Energy*, vol. 181, pp. 222–233, 2019.

[41] A. Sufyan, M. Jamil, S. Ghafoor et al., "A robust nonlinear sliding mode controller for a three-phase grid-connected inverter with an LCL filter," *Energies*, vol. 15, no. 24, pp. 9428–9516, 2022.

[42] K. Zeb, T. D. C. Busarello, and S. U. Islam, "Design of super twisting sliding mode controller for a three-phase grid-connected photovoltaic system under normal and abnormal conditions," *Energies*, vol. 13, pp. 1–20, 2020.

[43] S. Li, W. Chen, B. Fang, and D. Zhang, "A strategy of PI + repetitive control for LCL-type photovoltaic inverters," *Soft Computing*, vol. 24, no. 20, pp. 15693–15699, 2020.

[44] K. Deželak, P. Bracinik, K. Sredenšek, and S. Seme, "Proportional-integral controllers performance of a grid-connected solar PV system with particle swarm optimization and ziegler–nichols tuning method," *Energies*, vol. 14, pp. 1–15, 2021.

[45] K. Zeb, S. U. Islam, W. U. Din et al., "Design of fuzzy-PI and fuzzy-sliding mode controllers for single-phase two-stages grid-connected transformerless photovoltaic inverter," *Electronics*, vol. 8, no. 5, pp. 520–619, 2019.

[46] A. K. Zadeh, L. I. Kashkooli, and S. A. Mirzaee, "Designing a power inverter and comparing backstepping, sliding-mode and fuzzy controllers for a single-phase inverter in an emergency power supply," *Ciencia e Natura*, vol. 37, pp. 175–181, 2015.

[47] E. Kolbasi and M. Seker, "Nonlinear robust backstepping control method approach for single phase inverter," in *Proceedings of the 21st International Conference On Methods And Models In Automation And Robotics*, pp. 954–958, Miedzyzdroje, Poland, August 2016.

[48] S. Zouga, M. Benchagra, and A. Abdallah, "Backstepping control based on the pso algorithm for a three-phase pv system connected to the grid under load variation," in *Proceedings of the IEEE 4th International Conference on Electrical and Information Technologies (ICEIT')*, Rabat, Morocco, March 2020.

[49] M. F. Pervej, T. K. Roy, F. K. Tumpa, and M. I. Sarkar, "Nonlinear backstepping controller design for a three-phase grid-connected photovoltaic system using dpc approach," in *Proceedings of the 9th International Conference on Electrical and Computer Engineering (ICECE)*, pp. 407–410, Dhaka, Bangladesh, December 2016.

[50] T. K. Roy, M. A. Mahmud, A. M. T. Oo, and M. E. Haque, "Robust nonlinear adaptive backstepping controller design for three-phase grid-connected solar photovoltaic systems with unknown parameters," in *Proceedings of the IEEE Power and Energy Society General Meeting (PESGM)*, pp. 1–5, Boston, MA, USA, July 2016.

[51] T. K. Roy, M. A. Mahmud, and S. N. Islam, "Nonlinear backstepping controller design for grid-connected photovoltaic systems with output LC filters to improve dynamic stability and power quality," in *Proceedings of the IEEE International Conference on Power Electronics*, pp. 1–5, Cochin, India, January 2020.

[52] D. Xu, G. Wang, W. Yan, and C. Shen, "Nonlinear adaptive command-filtered backstepping controller design for three-phase grid-connected solar photovoltaic with unknown parameters," in *Proceedings of the Chinese Automation Congress (CAC)*, pp. 7823–7827, Jinan, China, October 2017.

[53] F. Liu, S. Duan, and P. Xu, "Design and control of three-phase pv grid connected converter with lcl filter," in *Proceedings of the IECON 2007-33rd Annual Conference Of the IEEE Industrial Electronics Society*, pp. 1656–1661, Taipei, Taiwan, March 2007.

[54] X. Bao, F. Zhuo, Y. Tian, and P. Tan, "Simplified feedback linearization control of three-phase photovoltaic inverter with an LCL filter," *IEEE Transactions on Power Electronics*, vol. 28, no. 6, pp. 2739–2752, 2013.

[55] D. Sgrò, S. A. Souza, F. L. Tofoli, R. P. S. Leão, and A. K. R. Sombra, "An integrated design approach of LCL filters based on nonlinear inductors for grid-connected inverter applications," *Electric Power Systems Research*, vol. 186, Article ID 106389, 2020.

[56] Y. Li, J. Zhang, Z. Hao, and P. Tian, "Improved pr control strategy for an lcl three-phase grid-connected inverter based on active damping," *Applied Sciences*, vol. 11, pp. 1–20, 2021.

[57] M. A. E. Alali and J.-P. Barbot, "A first order sliding mode controller for grid connected shunt active filter with a LCL filter," *IFAC-PapersOnLine*, vol. 50, no. 1, pp. 14812–14817, 2017.

[58] W. Xia and J. Kang, "Stability of LCL-filtered grid-connected inverters with capacitor current feedback active damping considering controller time delays," *Journal of Modern Power Systems and Clean Energy*, vol. 5, no. 4, pp. 584–598, 2017.

[59] M. Huang, Z. Zhang, F. Chen, W. Wu, Z. Yao, and F. Blaabjerg, "Stabilization design of three-phase LCL-filtered grid-connected inverter using IDA-PBC controller," *International Transactions on Electrical Energy Systems*, vol. 2022, Article ID 7515321, 14 pages, 2022.

[60] S. Vaidyanathan and A. T. Azar, *Backstepping Control of Nonlinear Dynamical Systems*, Academic Press, Cambridge, MA, USA, 2020.

[61] J. Yu, Y. Ma, H. Yu, and C. Lin, "Adaptive fuzzy dynamic surface control for induction motors with iron losses in electric vehicle drive systems via backstepping," *Information Sciences-Elsevier*, vol. 376, pp. 172–189, 2017.

[62] P. Giroux, G. Sybille, C. Osorio, and S. Chandrachood, "Detailed model of a 100-kw grid-connected pv array," *Hydro-Quebec and The MathWorks*, vol. 5, 2012.
[63] J. Qian, K. Li, H. Wu, J. Yang, and X. Li, "Synergetic control of grid-connected photovoltaic systems," *International Journal of Photoenergy*, vol. 2017, Article ID 5051489, 11 pages, 2017.
[64] D. Xu, G. Wang, W. Yan, and X. Yan, "A novel adaptive command-filtered backstepping sliding mode control for PV grid-connected system with energy storage," *Solar Energy*, vol. 178, pp. 222–230, 2019.
[65] T. K. Roy and M. A. Mahmud, "Active power control of three-phase grid-connected solar PV systems using a robust non-linear adaptive backstepping approach," *Solar Energy*, vol. 153, pp. 64–76, 2017.
[66] V. L. Nguyen, *Coupling photovoltaic systems and electric vehicles to the grid: problems and solutions*, University of Grenoble, Grenoble, France, Ph.D. Theses, 2014.